Available online at www.sciencedirect.com
SCIENCE DIRECT
Polymer 46 (2005) 6756–6766
polymer
www.elsevier.com/locate/polymer

Steady-state behavior of star polymers in dilute flowing solutions via Brownian dynamics

J.G. Hernández Cifre*, R. Pamies, M.C. López Martínez, J. García de la Torre

Departamento de Química Física, Facultad de Química, Universidad de Murcia, 30071 Murcia, Spain

Received 7 April 2005; received in revised form 3 June 2005; accepted 3 June 2005
Available online 19 July 2005

Abstract

A bead and spring model is considered for the Brownian dynamics simulation of the behavior of regular star polymer chains in a dilute solution under both shear flow and extensional (or elongational) flow. Finite extensibility, excluded volume, and hydrodynamic interaction are taken into account to make the polymer model as realistic as possible. The behavior of star-like chains in flow is similar to that of linear and ring polymers. Thus, dependence of a given property with the arm molecular weight is analogous to that found for linear polymers when using the total molecular weight. In shear flow, the deformation of the chain and the shear rate viscosity dependence (the flow curve), are studied. We find a slope for the shear-thinning region of the flow curve close to $-2/3$. In elongational flow the coil-stretch transition is characterized by giving the relationship between the critical elongational rate and the arm molecular weight, which turns out to be similar to the power law found in linear chains.

Keywords: Brownian dynamics; Bead-and-spring; Dilute solution

1. Introduction

Dynamics of flexible polymer chains in flowing solution is a topic widely studied by using computer simulation techniques, which allow to handle more sophisticated polymer models than those employed in analytical approaches. Most efforts have been devoted to solve conformational and dynamical problems of linear polymer under both shear and extensional flows.

In shear it is well known that polymer chains are oriented and deformed, which influences the solution flow properties, thus appearing the characteristic non-Newtonian behavior. Under extensional flows, flexible polymer chains experience the so-called coil-stretch transition [1,2], consisting of the abrupt, sudden, increase in polymer property values when the extensional rate exceeds a certain critical value. Previous papers of our group [3,4] are devoted to the study of such systems, and show the importance of the inclusion of effects such a excluded volume (EV) and hydrodynamic interaction (HI) in order to get results comparable to experiments.

In spite of the huge amount of work on flowing polymer solutions, less attention has been paid to polymers with non-linear topology, mainly to their behavior in extensional flows. In a previous paper [5], we simulated and analyzed the behavior of cyclic (ring) polymers under flow. Now, the present work extends the conclusions of the preceding one to another common topology, namely regular (uniform) star polymers. These are polymers with a single polyfunctional branching point, the central core, from which linear chains, so-called arms, of the same chemical structure and length stick out. They are, therefore, the simplest representatives of a wide class of branched polymers. Equilibrium and dynamics properties of star polymers have been characterized experimentally [6] and studied theoretically or with the help of computer simulations [7–10]. Very recent contributions to the study of conformational and hydrodynamic properties of star polymers are Refs. [11–13]. In this paper, we will not discuss equilibrium properties of star polymers but show their behavior under two typical flow situations: simple shear and steady uniaxial elongational flow. For this purpose we make use of the Brownian dynamics simulation technique (BD) including fluctuating hydrodynamic interaction.

* Corresponding author. Tel.: +34 968 367420; fax: +34 968 364148.
E-mail address: jghc@um.es (J.G. Hernández Cifre).

0032-3861/$ - see front matter © 2005 Elsevier Ltd. All rights reserved.
doi:10.1016/j.polymer.2005.06.058

2. Model and methodology

We consider a dilute solution of star polymers subjected to simple shear and uniaxial elongational flows. The velocity field of the shear flow is given by

$$v_x = \dot{\gamma} y, \quad v_y = 0, \quad v_z = 0 \tag{1}$$

whereas the elongational velocity field is given by

$$v_x = \dot{\varepsilon} x, \quad v_y = -\frac{1}{2}\dot{\varepsilon} y, \quad v_z = -\frac{1}{2}\dot{\varepsilon} z \tag{2}$$

where $\dot{\gamma}$ and $\dot{\varepsilon}$ are the shear and the elongational rate, respectively.

In shear flow it is convenient to use a dimensionless form of the shear rate related to the molecular weight of the polymer chain [14]

$$\beta = \frac{M\eta_s[\eta]_0}{N_A k_B T}\dot{\gamma} \tag{3}$$

where M is the molecular weight, η_s is the solvent viscosity, $[\eta]_0$ the zero-shear intrinsic viscosity, N_A the Avogadro number, k_B the Boltzmann constant and T the absolute temperature.

The polymer molecule is modeled as a bead-and-spring chain [14] with N beads connected by $N-1$ FENE (finite extensible non-linear elongational) springs which follow the force law [14]

$$\mathbf{F}^{(s)} = \frac{H}{1-(Q/Q_{max})^2}\mathbf{Q} \tag{4}$$

where $\mathbf{Q}$ is the spring vector, Q_{max} the maximum spring length and $H=3k_BT/b^2$ the spring constant, being b^2 the equilibrium mean squared length of a Hookean spring. If we define the chain length in terms of N_K Kuhn steps of length b_K, then $b^2 = N_K b_K^2$. Regular stars are formed by a central bead and F arms, the so-called functionality, of equal number of beads $N_{arm}=(N-1)/F$.

Intramolecular, excluded volume interactions to mimic solvent quality are simulated by introducing interaction forces between non-bonded beads. An adequate choice is the Lennard–Jones (LJ) potential

$$V = 4\varepsilon_{LJ}\left[\left(\frac{\sigma_{LJ}}{r_{ij}}\right)^{12} - \left(\frac{\sigma_{LJ}}{r_{ij}}\right)^{6}\right] \tag{5}$$

where r_{ij} is the distance between beads i and j and ε_{LJ} and σ_{LJ} are the Lennard–Jones parameters: Minimum energy and zero energy distance, respectively. As shown by Freire and co-workers, appropriate LJ parameter values that reproduce correctly the power laws relating polymer properties to molecular weight are $\varepsilon_{LJ}=0.1k_BT$ for good solvents [15] and $\varepsilon_{LJ}=0.3k_BT$ for theta solvents [16], with $\sigma_{LJ}=0.8b$ in any case. In this work we show mainly results obtained for polymers under good solvent conditions. In addition, some results corresponding to chains under theta conditions are also displayed to show their similar flow behavior with the good solvent case. Finally, simulations with chains in the absence of intramolecular potential between non-bonded beads, so-called 'phantom' chains and termed along the paper as ideal chains, were also carried out and results compared to those under good solvent conditions. A characteristic of ideal chains is the occurrence of unrealistic crossing of chain elements during the chain dynamics.

The dynamics of the polymer chain is monitored from trajectories of individual molecules obtained by BD simulation. We employ a predictor–corrector version of the Ermak and McCammon algorithm [17] proposed by Iniesta and García de la Torre [18]. Simulations with and without HI were performed. Fluctuating hydrodynamic interactions between beads are accounted for by means of the Rotne–Prague–Yamakawa tensor [19,20], as it has been done in most Brownian dynamics simulations of dilute polymer solutions [21]. This tensor includes terms of the orders -1 and -3 in the interbead distances, which usually suffices for the relatively open conformations of random coils. An exception could be, in our case, the star core having high density of segments for which improved representations of HI would be more accurate [22,23]. As this dense region has a low mobility, we expect that the effect of the more intense HI at the core will have a minor influence in the results for the overall properties. For the bead friction we use a Stokes coefficient $\zeta=6\pi\eta_s\sigma$, where $\sigma=0.257b$, which correspond to a dimensionless HI parameter $h^*=0.25$. In this way, five independent polymer trajectories are generated. Steady-state properties are computed by averaging over each trajectory, after discounting the initial part for equilibration purposes. Then, the mean and standard deviation over the five trajectories are taken to characterize the actual property values.

Along the work, quantities are given in the following unit system: b, k_BT and $\zeta b^2/k_BT$, which are the units for length, energy and time, respectively. For simplicity, we will not use any special notation to indicate dimensionless quantity. In the unit system employed, the spring constant becomes $H=3$ and the maximum spring length $Q_{max}=10$. The simulation time step was $\Delta t=10^{-4}$, as required when the Lennard–Jones potential is present in the computation.

3. Results

3.1. Shear flow

We study the influence of the shear rate β on the star dimensions in terms of the parameters δ^2, δ_{xx} and δ_{yy} which give, respectively, the relative increase in the mean-square radius of gyration

$$\delta^2 = \frac{\langle s^2\rangle}{\langle s^2\rangle_0} - 1 \tag{6}$$

and the relative increase in the components of the radius of gyration along the flow direction

$$\delta_{xx} = \frac{\langle G_{xx}\rangle}{(1/3)\langle s^2\rangle_0} - 1 \tag{7}$$

and along the gradient direction

$$\delta_{yy} = \frac{\langle G_{yy}\rangle}{(1/3)\langle s^2\rangle_0} - 1 \tag{8}$$

The gyration tensor is defined as $\mathbf{G} = [1/(2N^2)]\sum_{i=1}^{N}\sum_{j=1}^{N}\langle \mathbf{r}_{i,j}\mathbf{r}_{i,j}\rangle$, where $\mathbf{r}_{i,j}$ is the vector between beads i and j. We also study the influence of the shear rate on the intrinsic viscosity

$$[\eta] = -\frac{N_A}{\eta_s n M}\frac{(\tau_{xy})_p}{\dot{\gamma}} \tag{9}$$

where n is the number concentration of polymer and $(\tau_{xy})_p$ the polymer contribution to the shear stress. For a bead-and-spring macromolecular model with N beads, the polymer contribution to the stress tensor is calculated using the modified Kramers expression [14] which, neglecting the isotropic part, reads

$$\tau_p = n\sum_{i=1}^{N}\langle \mathbf{R}_i\mathbf{F}_i\rangle \tag{10}$$

where $\mathbf{R}_i$ is the position vector of bead i respect to the center of mass of the chain and $\mathbf{F}_i$ is the net force exerted on bead i by springs and excluded volume interactions. The brackets $\langle\,\rangle$ mean conformational average.

Fig. 1(A) shows the evolution of δ^2 with β for various star molecular weights, N, in good solvent conditions ($\varepsilon_{LJ}=0.1$) and with HI, but keeping fix the number of arms, $F=4$ and, therefore, varying N_{arm}. For the sake of clarity vertical error bars are displayed in figures when they are bigger than the symbol size used. The aspect of those plots are similar to that for linear and ring chains with both FENE and Hookean springs [3,5]. Thus, at low and moderate shear rate, δ^2 follows a straight line in a log–log plot. Besides, values of δ^2 for different N tend to superimpose, since β makes results molecular weight independent at low and intermediate shear rates. At high shear rate, however, a downward curvature appears when FENE chains are employed (black symbols) as a consequence of the finite extensibility of the chain, and δ^2 values start to slightly differ, increasing with the number of beads, N. At extremely high shear, chains are completely unraveled and stretched and values of δ^2 will tend to a constant value consistent with the full elongation of the chains. Clearly, when Hookean chains are used (empty symbols), deformation can increase infinitely so that the linearity of the plot is extended to large β values. Thus, a good estimate of the slope can be obtained by using Hookean springs because this model presents the same asymptote than that predicted with FENE springs at low values of β. The dependence in the linear part of the curve, can be expressed by a power law,

$$\delta^2 = C\beta^a \tag{11}$$

For the case of Gaussian chains with HI presented in Fig. 1(A), we obtain an exponent $a=2.14\pm0.04$. Thus, the power law found for linear chains, $\delta^2=C\beta^2$ [3], holds also in the case of star chains. For FENE chains, we find an exponent slightly lower (about 1.8), although the downward curvature at high shear due to the finite extensibility makes difficult to evaluate precisely the slope of the linear region. The β dependence of δ^2 at the intermediate shear rate, where HI and EV start to gradually vanish, is a reflection of the complex interplay of both effects. Their influence on the exponent of Eq. (11) has been evaluated for linear chains in Refs. [24–26] and for ring polymers in our previous paper [5]. Fig. 1(B) and (C) represents the deformations along the flow (δ_{xx}) and gradient (δ_{yy}) direction, respectively, the latter being a semilog plot. As appreciated, the chain stretches along the flow direction much more than it compresses in the perpendicular direction. Thus, the value of δ_{yy} decreases slightly with the flow, whereas δ_{xx} increases several orders of magnitude. Again (Fig. 1(B)), it can be appreciated that at high shear, in the non-linear region, the star with higher N presents a higher value of the deformation along the flow direction. The value of the slope of the linear region is about 1.8 as that found for δ^2. Clearly, the overall deformation, δ^2, coincides with the x-component under large shear.

In Fig. 2 we set $N=25$ and vary the number of arms, F. As appreciated the different plots do not superimpose and the intercept, related to the constant C in Eq. (11), is clearly different. Obviously, in increasing F keeping N, the number of beads per arm, N_{arm} (equivalently the number of beads of the larger linear piece of the chain, $2N_{arm}+1$) decreases and so does the 'deformability' of the polymer. Furthermore, the bead density in the star core is higher and the star becomes closer to a rigid sphere. It means that deformation, a relation between equilibrium and non-equilibrium size, is smaller for identical dimensionless shear rate, β. Thus, the upper limiting value of δ^2 corresponds to that of the linear chain ($F=2$), as appreciated in the mentioned figure. However, the slope of the linear part of the curve, i.e. the exponent of the Eq. (11), is practically independent of the functionality. At very large β, the fully elongated arms cluster in opposite directions respect to the central bead giving rise to a rod-like conformation along the flow and, therefore, the F dependence becomes weak.

Finally for the sake of completeness, we compare in Fig. 3 the shear evolution of the deformation for stars with identical N_{arm}, therefore, different N and F but identical larger linear piece. We also include the corresponding linear polymer ($F=2$) with $N=2N_{arm}+1$. We will see later the relevance of the arm molecular weight to characterize the star behavior, mainly under elongational flow. Ideal chains are used here because we dispose of much more results for this kind of chains. Curves clearly do not superimpose in the linear region. As before, geometries closer to a rigid sphere, i.e. higher value of F, are observed to present smaller values

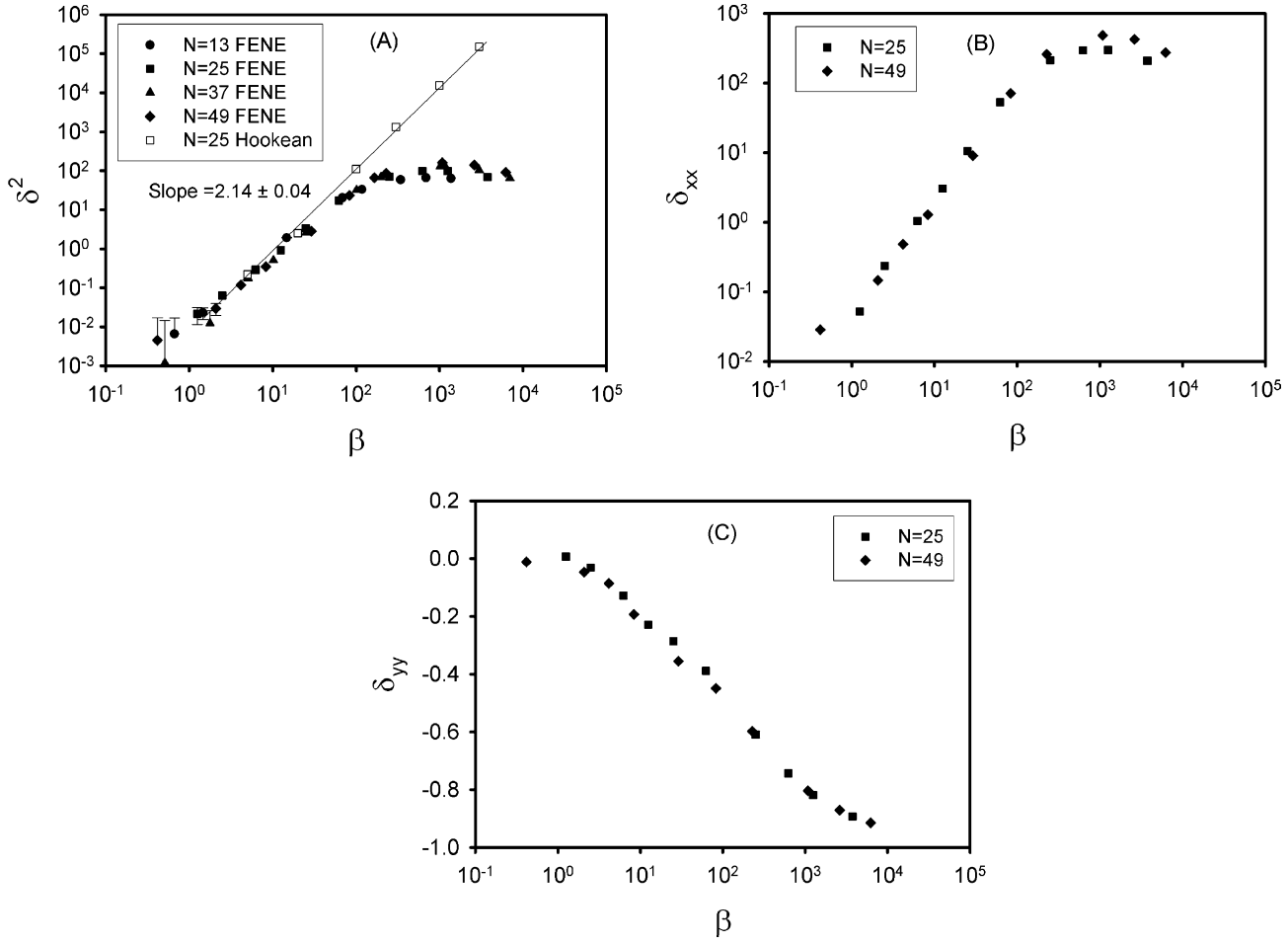

Fig. 1. (A) Dependence of the star deformation, δ^2, on the shear rate, β, for several N and fixed $F=4$. (B) Dependence of δ_{xx} of stars with $F=4$ on β. (C) Semilog plot of the dependence of δ_{yy} of stars with $F=4$ on β. All simulations include HI and LJ potential (good solvent).

of δ^2. The slope of the linear part is again approximately 2. All curves tend to superimpose in the final non-linear region, where chains are in their fully elongated rod-like conformations. Clearly, because N_{arm} is the same, the maximum deformation of these FENE chains is practically identical.

Fig. 4(A) shows the shear rate evolution of the intrinsic viscosity (relative to its zero-shear value) of star polymers

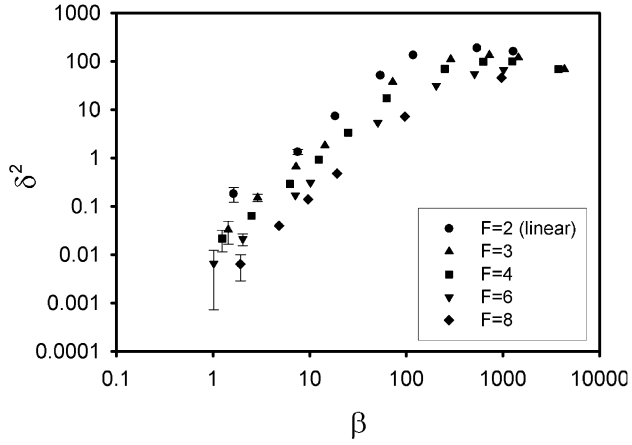

Fig. 2. Dependence of the star deformation, δ^2, on the shear rate, β, for several F and fixed $N=25$. All simulations include HI and LJ potential (good solvent).

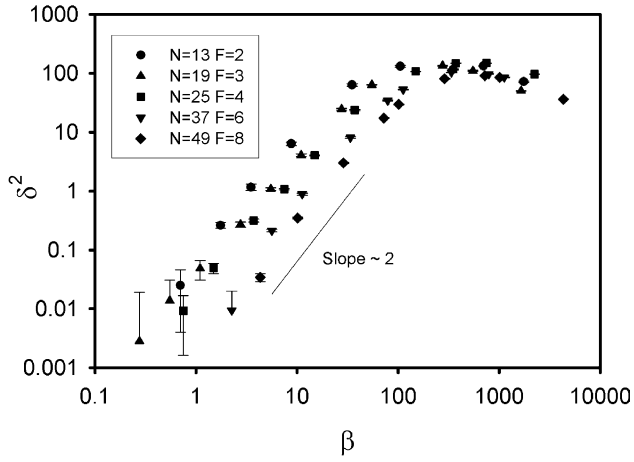

Fig. 3. Dependence of the star deformation, δ^2, on the shear rate, β, for fixed $N_{arm}=6$. All simulations with HI and without LJ potential (no-EV, ideal chains).

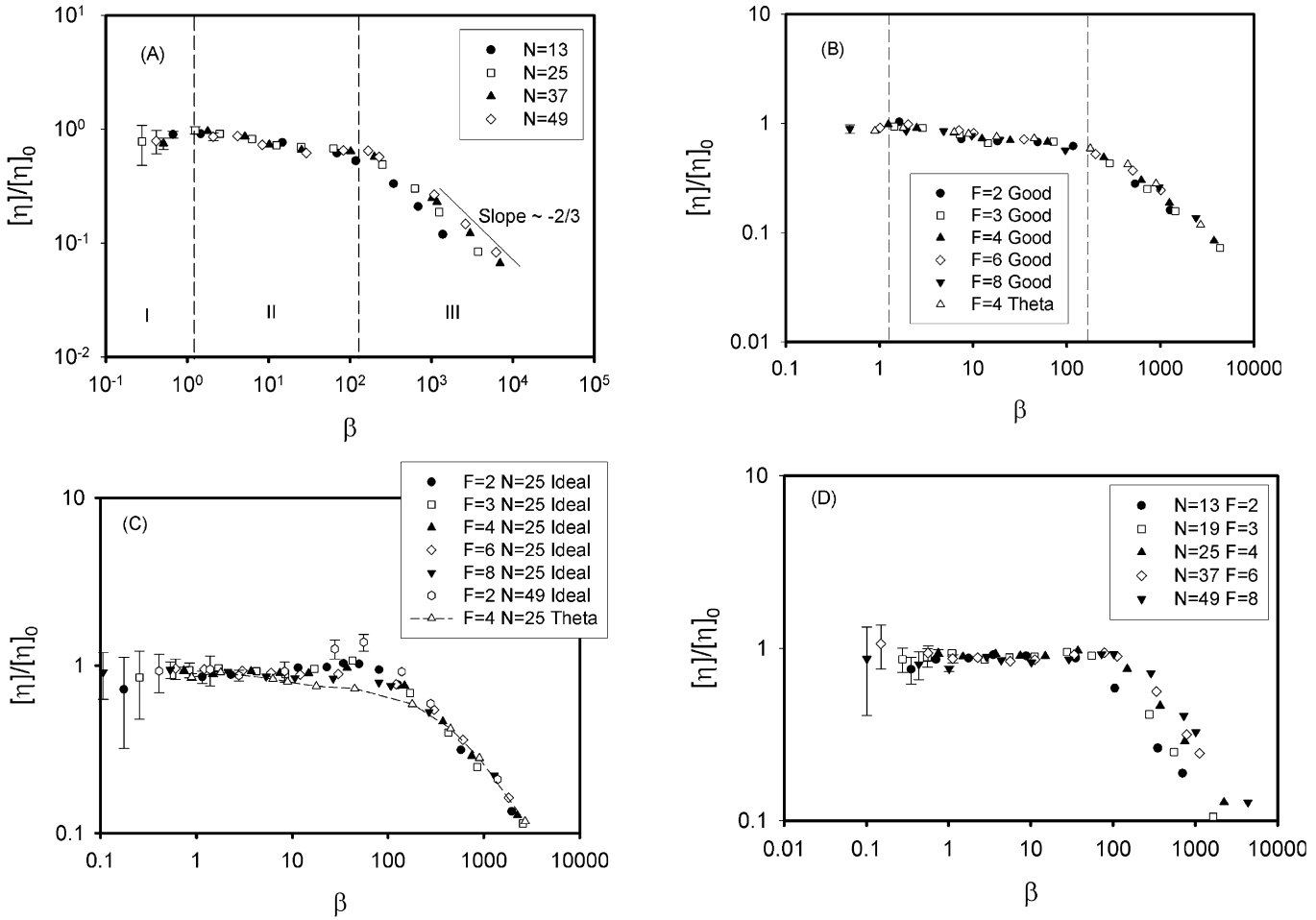

Fig. 4. Relative intrinsic viscosity, $[\eta]/[\eta]_0$, vs. β of stars: (A) several N, fixed $F=4$, HI and LJ potential (good solvent); (B) several F, fix ed $N=25$, HI and LJ potential (good and theta); (C) several F, $N=25$ and 49, HI, ideal (no-EV). Extra points of $N=25$ theta; (D) Fixed $N_{arm}=6$, HI and no-EV.

of several N, fixed $F=4$, with HI and in good solvent conditions. As expected, β makes $[\eta]/[\eta]_0$ values N independent as long as the shear rate is not very high. The viscosity curve presents three different regions. Region I is the Newtonian plateau, characteristic at low shear rate ($\beta \lesssim 1$ in our plots). Region III is the shear-thinning region, characteristic of most macromolecular fluids, where viscosity decreases strongly with shear rate. This non-linearity arises because molecules are highly oriented along the flow direction and close to fully stretched, therefore, being a direct consequence of the finite extensibility. As observed, points corresponding to different N clearly do not superimpose, the discrepancy in the value of $[\eta]/[\eta]_0$ being more noticeable in diminishing N (equivalently N_{arm}). By using the three last points of the curves in the shear-thinning region we calculate a slope of -0.73 ± 0.04 for $N=13$ and -0.663 ± 0.04 for $N=49$. Thus, $[\eta]/[\eta]_0$ is a bit lower as N is smaller (for a given β). However, it must be noticed that the zero-shear intrinsic viscosity, $[\eta]_0$, used to compute β, depends on the HI and EV effects included in our simulations, which disappear at very high shear and, therefore, in that region we are not employing the most appropriate value of β to get N-independent behavior. In any case, the slope of the shear-thinning appearing in the log–log plots obtained from our simulations, although slightly varying with N, are close to the value $-2/3$ found theoretically in Ref. [27]. A slope smaller (in absolute value) than -1, the upper limit of the FENE spring model, is also in good agreement with experiments. However, experiments usually do not reach so large shear rates, since flow instabilities start to appear. Finally, an interesting part is region II, which could be termed as 'pseudo-plateau'. There, the viscosity presents an ondulation. Thus, it diminishes slightly with β, and then increases a bit, appearing a shear-thickening behavior, before the clear shear-thinning region. This kind of behavior is due to the influence of EV and HI at the intermediate shear rate region as predicted theoretically [27] and found in previous simulations of our group using other topologies [5,28].

Fig. 4(B) corresponds to the same kind of representation as Fig. 4(A) but keeping $N=25$ and varying F in order to show the influence of the functionality. The three above-mentioned regions are again appreciated. Since N is kept fixed, different curves apparently superimpose quite well, mainly at low β. In the strong shear-thinning region points tend to diverge, $[\eta]/[\eta]_0$ (for a given β) becoming slightly higher in increasing F. This can be expected, since at smaller F (and large N_{arm}) chains present less spherical (more rod-like) symmetry and they are better oriented along the flow resulting in an easier shear viscosity decrease relative to its zero-shear value. Slopes are again about -0.7, decreasing slightly (in absolute value) with increasing F. Some points corresponding to the simulation of a star with $F=4$ under theta conditions ($\varepsilon_{LJ}=0.3$) were included. As observed, points superimpose well (recall that viscosities are normalized to the zero-shear value) showing a flow behavior similar to that of good solvent condition ($\varepsilon_{LJ}=0.1$).

In Fig. 4(C) we switch the LJ potential off (except in one case) by using ideal chains and keep the HI effect. Thus, the influence of HI in the intermediate shear rate region is better appreciated. Now, intrinsic viscosity behaves Newtonian at low shear, without the ondulation appreciated in Fig. 4(B), due to the absence of EV (see Ref. [28] for a deeper discussion on the effects of EV and HI). However, prior to the sharp shear thinning a shear-thickening region appears as a consequence of the stretching of the arms and the subsequent weakening in HI, as predicted theoretically [27]. Chains without HI are less protected against the flow, presenting a higher friction and thus a higher viscosity. This shear thickening is stronger as N_{arm} is larger and the unraveling of the chain produces a more dramatic effect on the HI decrease (i.e. chain becomes more free-draining, thus increasing the viscosity). Furthermore, higher F and shorter arms implies a more dense core, and HI effect does not disappear easily. In Fig. 4(C) points corresponding to a larger linear chain with $N=49$ were added to better show the importance of the arm molecular weight on the value of the maximum. Thus, shear thickening is slightly stronger for chains with $F=2$, whereas chains with short arms do not present that maximum. Again, all points superimpose quite well up to the shear-thickening region. Besides, points corresponding to the case $N=25$ and $F=4$ under theta solvent condition (empty up-triangles crossed by dashed line) were added to show that the flow behavior of ideal and theta chain models are not equivalent. The inclusion of intramolecular LJ potential, regardless good or theta conditions produces the same effect of diminishing the intrinsic viscosity with shear and, therefore, tends to suppress the shear thickening. Finally, in the shear thinning region slopes are again, as in Fig. 4(B), slightly different and about -0.7. The functionality independence of $[\eta]/[\eta]_0$ at low β implies that, at least in that region, the ratio of the intrinsic viscosity of a star, $[\eta]_s$, to that of the corresponding (same N) linear polymer, $[\eta]_l$, has the same value as the ratio of their zero-shear intrinsic viscosities measured at the same β: $[\eta]_s/[\eta]_l=[\eta]_{0,s}/[\eta]_{0,l}$.

Finally, in Fig. 4(D) we compare the viscosity behavior of stars with the same arm molecular weight, i.e. the same larger linear piece of chain, $2N_{arm}+1=13$. We present results for chains without intramolecular excluded volume potential. As appreciated, in the Newtonian plateau region all data of the relative intrinsic viscosity superimpose quite well. In the case shown, shear thickening is hardly appreciated because chains are too short and the decrease of the HI effect is not relevant (notice that this case corresponds to the case $F=4$ in Fig. 4(C)). In the shear-thinning region results for each case now clearly diverge and the onset of the decay appears at smaller β in decreasing F and N. Since N_{arm} is constant, $[\eta]/[\eta]_0$ must be higher as the star approaches the rigid sphere limit, i.e. in increasing

F, and arms cluster less easily to form a rod-like conformation.

Although this paper is focused on the flow behavior of regular stars, it is worth mentioning that the numerical results obtained in the absence of flow, $\langle s^2\rangle_0$ and $[\eta]_0$ (employed here to get the relative quantities δ^2 and $[\eta]/[\eta]_0$), agree qualitatively well with experimental results reported in Ref. [6] for the zero-shear molar mass dependence of those star quantities. In both cases there exist power relationships of the radius of gyration and the intrinsic viscosity with the molecular weight, N. Furthermore, as the molecule presents a higher spherical symmetry (same molecular weight but higher functionality) both the intrinsic viscosity and the radius of gyration decrease their values, resulting log–log plots for $\langle s^2\rangle_0$ and $[\eta]_0$ parallel to those of their linear counterparts [6]. Clearly, in diminishing the arm dimensions and increasing the spherical symmetry the zero-shear intrinsic viscosity will be smaller. A different situation occurs under strong shear flow. In such a case, as explained previously (Fig. 4(B)), molecules that are able to rearrange their overall shapes and align easily with the flow (i.e. stars with small F) will undergo a higher decrease of the intrinsic viscosity respect to their zero-shear value, in spite of their higher deformation (Fig. 1(A)).

3.2. Extensional flow

When flexible polymers are subjected to an elongational rate of strain greater than a certain threshold value they experience an abrupt increase in their conformation dependent properties due to the sudden unraveling of the random coil [2,4]. In this paper we are concerned with the dependence of the average steady-state properties of star-like chains on the elongational rate. This kind of study allows for the determination of the critical elongational strain rate value, $\dot{\varepsilon}_c$.

In Fig. 5(A) results for the steady-sate values of the mean square radius of gyration, $\langle s^2\rangle$, as a function of $\dot{\varepsilon}$ are plotted. There, the coil-stretch phenomenon for regular star chains of 25 beads with HI in good solvent conditions and with different number of arms, F, is clearly illustrated. The coil-stretch transition is seen as a large, sudden increase in $\langle s^2\rangle$ at a certain value of the elongational rate $\dot{\varepsilon}_c$ marked in plots of Fig. 5(A) with dotted lines. Thus, at $\dot{\varepsilon} < \dot{\varepsilon}_c$ chains stay near their equilibrium coil conformations. As appreciated, curves shift to the right, i.e. greater $\dot{\varepsilon}_c$, as the functionality, F, increases. This is because higher F implies smaller N_{arm} and the critical elongational rate of stars depends mainly on the molecular weight of their largest linear piece, analogously to linear polymers for which $\dot{\varepsilon}_c$ decreases with chain molecular weight. In the low flow rate region of Fig. 5(A) ($\dot{\varepsilon} \ll \dot{\varepsilon}_c$) it is also observed that stars with more arms, therefore, shorter arms, present a smaller $\langle s^2\rangle$, as expected. In addition, it seems (see region around $\dot{\varepsilon}_c$) that the coil-stretch transition is sharper as N_{arm} increases and the star is closer to the linear topology. Finally, as explained in the

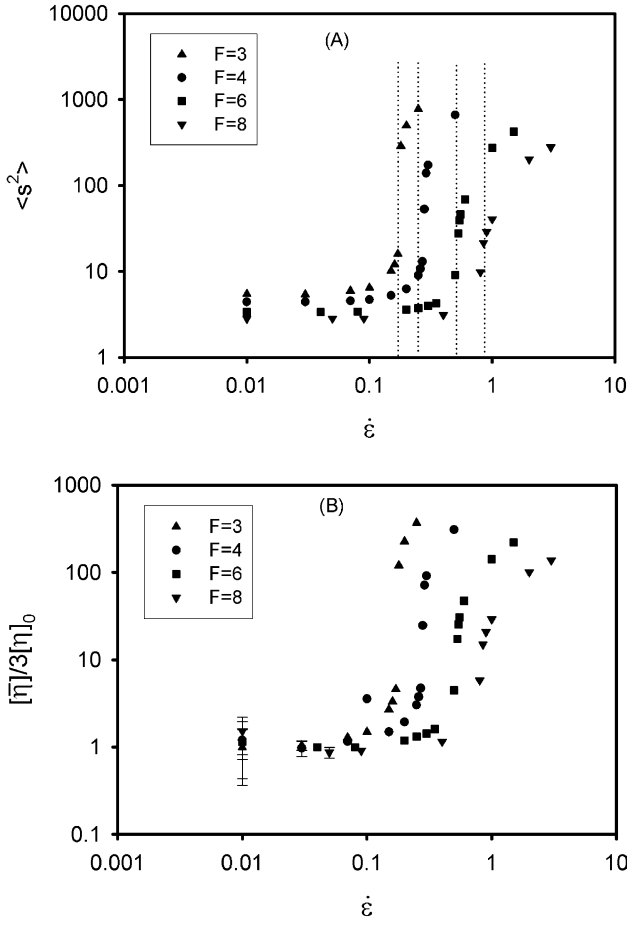

Fig. 5. Elongational rate dependence of (A) the mean squared radius of gyration, $\langle s^2\rangle$ and (B) the elongational intrinsic viscosity (normalized to its equilibrium value), for stars with $N=25$, varying F and with HI and LJ potential (good solvent).

previous section, at very high flow rates the curve tends to reach a plateau when FENE springs reach their maximum elongation. In Fig. 5(B) the ratio of the elongational intrinsic viscosity, $[\bar{\eta}]$, to its equilibrium value $3[\eta]_0$, $[\eta]_0$ being the zero-shear intrinsic viscosity (Trouton relation), is represented versus the elongational rate of strain. The elongational intrinsic viscosity is defined as

$$[\bar{\eta}] = -\frac{N_A}{\eta_{sn}M}\,\frac{\tau_{xx}-\tau_{yy}}{\dot{\varepsilon}} \tag{12}$$

where τ_{xx} and τ_{yy} are the normal components of the stress tensor, parallel and perpendicular to the flow, respectively. The polymer contribution to the components of the stress tensor is computed according to Eq. (10). As observed, at low $\dot{\varepsilon}$ the elongational viscosity is independent of the flow rate, as it corresponds to the Newtonian regime. However, at $\dot{\varepsilon} \geq \dot{\varepsilon}_c$ the viscosity increases abruptly, analogously to the radius of gyration, giving the characteristic elongational–thickening behavior of polymer solutions.

Fig. 6 shows the same kind of dependence that Fig. 5(A) but now for chains with identical functionality, $F=6$, and different molecular weight, N. These chains again present

different arm molecular weight and, therefore, different $\dot{\varepsilon}_c$, which shifts to higher values as N_{arm} diminishes. In this plot, it is clearly appreciated how chains with higher N and, therefore, higher N_{arm} present higher $\langle s^2 \rangle$ equilibrium value. Points corresponding to the case $N=25$ in theta conditions were also plotted (empty circles). As observed, they superimpose well with the corresponding points for good conditions mainly from $\dot{\varepsilon}_c$ on since chains are stretched and intramolecular LJ potential is not relevant. At $\dot{\varepsilon} < \dot{\varepsilon}_c$ values of $\langle s^2 \rangle$ at theta conditions are obviously somewhat smaller than those in good solvent although the log scale makes it difficult to appreciate. Fig. 7 shows the flow dependence of $\langle s^2 \rangle$ for several chains with the same $N_{arm}=6$, including the case of linear chain ($F=2$ and $N=13$). As it is clearly appreciated all the plots superimpose well about the same value of $\dot{\varepsilon}_c$, as indicated by the dashed line. That plot corroborates the above mention finding, e.g. the critical elongational rate depends on the arm molecular weight. Furthermore, the value of $\dot{\varepsilon}_c$ of a linear chain with N beads is very similar to that of a star chain with the same longest linear piece (i.e. with $2N_{arm}+1=N$). At $\dot{\varepsilon} < \dot{\varepsilon}_c$, i.e. at and near equilibrium, dimensions of the chain increase with F, i.e. as the overall shape of the star is more spherical (recall that N_{arm} is constant). Some points obtained from simulations both under theta and ideal (no-LJ) conditions (empty symbols) are also shown. Clearly, dimension of ideal chains at low elongational rate diminishes respect to its value for the analogous chains with intramolecular LJ potential, nevertheless the value of $\dot{\varepsilon}_c$ is not significantly influenced.

As observed in Figs. 5(A) and (B), 6 and 7, the value of the critical elongational rate is strongly dependent on the arm molecular weight, N_{arm}, but not on the total molecular weight or the functionality separately. Besides, $\dot{\varepsilon}_c$ depends on the presence or absence of HI, as discussed in our previous paper [4], where the power law relating the critical rate to the polymer molecular weight for linear chains was determined. It is then the purpose of the last part of this paper to study the corresponding scaling relationship arising for star polymers.

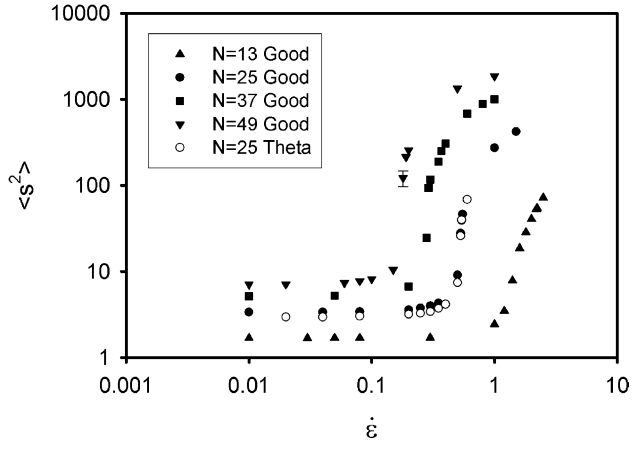

Fig. 6. Elongational rate dependence of $\langle s^2 \rangle$ for stars with varying N, fixed $F=6$ and with HI and LJ potential (good and theta).

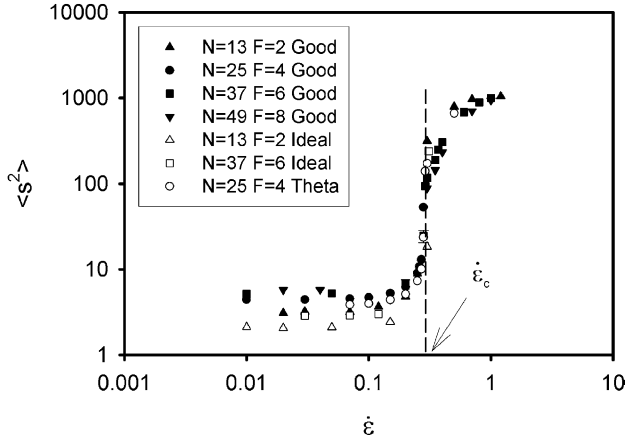

Fig. 7. Elongational rate dependence of $\langle s^2 \rangle$ for stars with fixed $N_{arm}=6$, HI and both LJ potential (good and theta) and no-EV (ideal).

The strong effect of the coil-stretch transition on polymer properties makes the value of $\dot{\varepsilon}_c$ easily computable. The procedure followed to determine $\dot{\varepsilon}_c$ of FENE ring polymers in our previous paper [5] was employed again in this work. In Ref. [5], we considered that the transition takes place as soon as the radius of gyration reaches fifty times its equilibrium value, $s^2_{trans} = 50 s^2_0$. The transition is so sharp, that several criteria can be used without influence on the critical value obtained. Fig. 8 shows, in a log–log plot, the scaling relationships between $\dot{\varepsilon}_c$ and N_{arm} for regular stars. A given N_{arm} value can be obtained with several combinations of N and F, nevertheless all of them yield about the same value of $\dot{\varepsilon}_c$. Both free-draining (no HI) and non-free draining (HI) chains were considered. As appreciated, the slope depends strongly upon the inclusion of HI effect. Nevertheless the inclusion of intramolecular Lennard–Jones potential to represent good or theta solvent conditions or the absence of it (ideal chain) seems to be

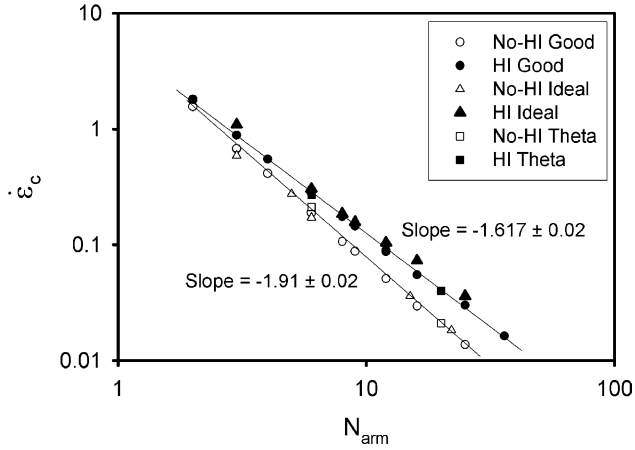

Fig. 8. Dependence of the critical elongational rate, $\dot{\varepsilon}_c$, with the star arm molecular weight, N_{arm}. Cases with HI, no-HI, LJ potential (good and theta) and no-EV (ideal) are considered.

irrelevant, i.e. the power law exponent is invariant respect to the solvent quality as found in other simulations and experiments (see Refs. [2,29–31] and our previous works with linear and ring topologies [4,5]). In the absence of HI, the slope in the log–log plot is about −2, more exactly we get the relationship $\dot{\varepsilon}_c = (5.9 \pm 0.2) N_{arm}^{(-1.91\pm0.02)}$, in good agreement with the well-known theoretical quadratic power law governing free-draining linear chains. Forcing the exponent to be −2, we get

$$\dot{\varepsilon}_c = 6.9 N_{arm}^{-2} \tag{13}$$

Notice that, if expressed in terms of the longest linear sequence in the star chain, i.e. $2N_{arm}+1 \simeq 2N_{arm}$ (for large enough arms), the numerical factor in Eq. (13) becomes ~27.6, very close to the constant $3\pi^2 = 29.6$ predicted theoretically for linear chains [4].When HI is considered it seems that the slope in the log–log plot takes values between −1.5 and −1.6. Indeed, to be precise, our simulation results with HI and EV (good solvent), can be adjusted to the equation $\dot{\varepsilon}_c = (5.1 \pm 0.2) N_{arm}^{-1.617\pm0.019}$, whereas our results with HI and ideal chains can be fit to $\dot{\varepsilon}_c = (5.5 \pm 0.7) N_{arm}^{-1.57\pm0.06}$. Points obtained for chains in theta conditions seem to superimpose well with those of good solvent, as already found for linear and ring chains [4,5]. Difference in exponent due to the inclusion or not of LJ potential is small so that, within the error, the way of representing the solvent quality can be considered to have no influence on the scaling relationship. Discrepancies may be because values of N, or more precisely values of N_{arm}, are not large enough to be in the long chain limit and the core can have some influence. Noticeably, an exponent of −1.6 agrees well with the theoretical predictions of Rabin and co-workers for linear chains in good solvent [32]. Furthermore, in our previous works with both linear [4] and ring [5] chains we found an exponent of -1.55 ± 0.03 that could also be well approximated to −1.6. If we force the exponent of the power law of the HI and EV case to be −1.6, we get

$$\dot{\varepsilon}_c = 5.0 N_{arm}^{-1.6} \tag{14}$$

in which case, using the same argument as for no-HI, in terms of $2N_{arm}$ the numerical factor in Eq. (14) becomes $5.0 \times 2^{1.6} \simeq 15.1$. However, quite accurate experiments to determine the critical strain rate of flexible linear polymers in elongational flow [29] report an exponent value of −1.5. If we force the exponent to be exactly −1.5 (as we did in Refs. [4,5]), we get

$$\dot{\varepsilon}_c = 4.1 N_{arm}^{-1.5} \tag{15}$$

in which case, in terms of $2N_{arm}$ the numerical factor in Eq. (15) becomes $4.1 \times 2^{1.5} \simeq 11.6$, in good agreement with the constant 11.7 found in Ref. [4] for linear chains (which were forced to scale as $N^{-1.5}$). In conclusion, scaling relationships between the critical elongational rate and molecular weight for regular star chains are analogous to those found for linear and ring chains [4,5] just changing the total molecular weight, N, by the arm molecular weight, N_{arm}.

In a previous work [4] we combined the value of the critical elongational rate, $\dot{\varepsilon}_c$, and the longest viscoelastic relaxation time (related to birefringence and viscosity relaxations), τ_1, of linear chains with the same N, to get the dimensionless quantity, $\dot{\varepsilon}_c \tau_1 = 0.50$. That quantity, ratio of a characteristic time of the molecule to a characteristic time of the experiment (inverse of the strain rate) is the so-called Deborah number, De. Analogously, we can combine the value of $\dot{\varepsilon}_c$ and τ_1 for regular stars with the same N_{arm}. Rey et al. [7] found $\tau_1' = 0.26 N_{arm}^{1.5}$ for regular stars with HI and without EV. The time τ_1', obtained from the correlation function of the first Rouse mode, is the longest relaxation time related to dielectric relaxation, which is related to the longest viscoelastic relaxation time by $\tau_1 = \tau_1'/2$ and, therefore, $\tau_1 = 0.13 N_{arm}^{1.5}$. This leads after Eq. (15) (considering that EV is not relevant) to $\dot{\varepsilon}_c \tau_1 \approx 0.5$. We made simulations (not shown here) to get values of τ_1 from the decay of birefringence and radius of gyration of stars with HI and EV. Again, we obtain $\dot{\varepsilon}_c \tau_1 \approx 0.5$, as it was the case for linear chains. Therefore, in experiments of polymers in elongational flow, the Deborah number must reach the threshold value De = 0.5 in order the coil-stretch transition to occur. This seems to be a universal value in the sense that it is independent of the topology of the chain. Furthermore, our simulations using a non-trivial chain model with non-linear geometry validate the well-known prediction based on the Hookean dumbbell model about the existence of an abrupt stretching of the polymer chain when De = 0.5 [14]. Nevertheless, the singularity that appears in using the Hookean dumbbell model and the subsequent infinite chain dimensions predicted theoretically are unrealistic.

4. Spring lengths under flow

Finally, it is interesting to notice that simulations results agree with the notion that tension accumulates at the central springs [27]. Thus, the most elongated springs are connected to the branch point, tension increasing from the free ends towards the core. Fig. 9(A) and (B) show the average length of each spring according to its position along the arm (starting from the core) for chains with $N = 25$, HI, both good and ideal conditions and with several functionalities, F (thus in increasing F the number of springs per arm diminishes). The mean length of star segments as a function of their position from the core was computed averaging over the trajectory and over the arms of the star provided we checked that springs in a given position presented similar mean length irrespective the arm.

At quiescent solution and at low flow intensity, i.e. when the chain is near the random coil conformation (Fig. 9(A)), it is observed that, under good solvent conditions, all central springs of a given arm present a similar average length, regardless its functionality and the type of flow employed,

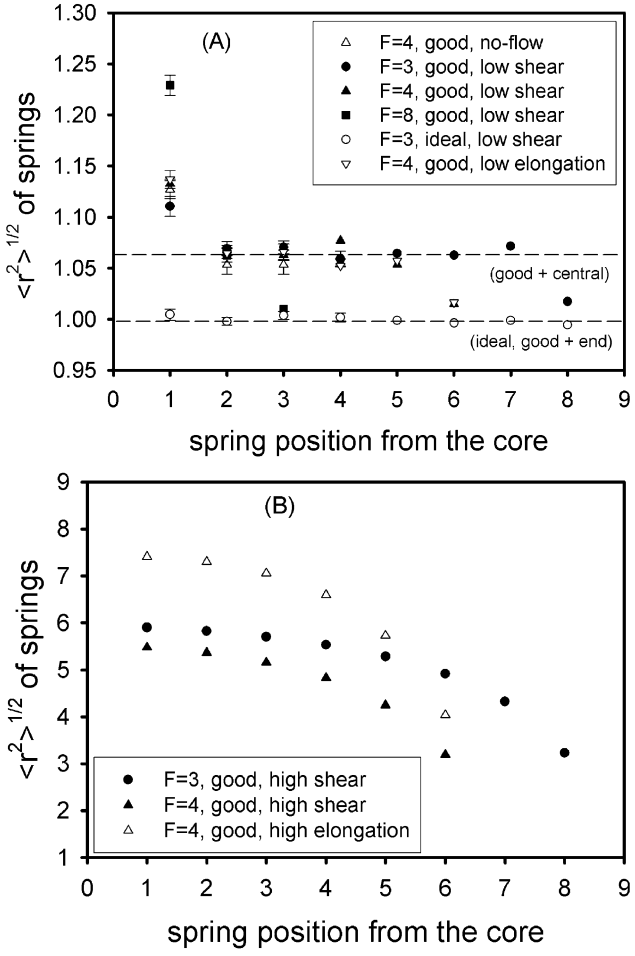

Fig. 9. Dependence of spring lengths on position along the arm for stars with $N=25$ and several F, under both shear and elongational flow. Cases with HI, LJ potential (good) and no-EV (ideal) are considered. (A) Low flow intensity ($\beta \leq 2$, $\dot{\varepsilon} < \dot{\varepsilon}_c$). (B) High flow intensity ($\beta > 200$, $\dot{\varepsilon} > \dot{\varepsilon}_c$).

whereas the spring attached to the core present a larger length and the end spring a shorter one. Because chains are at or near equilibrium, spring dimensionless lengths are about 1. Dashed lines of Fig. 9(A) and their labels can help to guide the eye and summarize the conclusions given here. We also observe that F influences the spring length attached to the core which is more elongated as F is higher since it is connected to more springs, carrying a higher tension. Clearly as the core density is higher, core springs stretch out as required by excluded volume interactions. This is clearly appreciated in the chain with $F=8$ (black squares) which has three springs per arm. The core (first) spring is quite stretched, the length of the central (second) one superimpose with that of the second spring of stars with $F=3$ and 4 (recall we are discussing the good solvent case), and the length of the end (third) spring is similar to that of the end springs of chains with $F=3$ (eighth spring, black circles) and $F=4$ (sixth spring, triangles). Furthermore, the length of these free end springs is practically that of equilibrium: 1. On other hand, all springs of an ideal chain (empty circles) have about the same length regardless their position in the arm and the type of flow, since beads can overlap and tension can relax easily. Spring lengths of ideal chains are exactly 1, smaller than under good solvent as chain is not expanded due to excluded volume.

Fig. 9(B) shows the effect of both shear and elongational flows on spring lengths of chains with $N=25$, $F=4$, HI and good solvent conditions. Flow intensities were chosen high enough so that chains are far from their equilibrium random coil conformation: in shear flow β belongs to the shear-thinning region and in elongational flow $\dot{\varepsilon} > \dot{\varepsilon}_c$. In the case of elongational flow, rate of strain was more than twice its critical value so that all arms were clearly stretched and aligned along the flow (if $\dot{\varepsilon} \approx \dot{\varepsilon}_c$ not all arms are similarly stretched). As observed in Fig. 9(B), under such flow intensities springs lengths can reach several times the dimensionless equilibrium length 1. In any case, spring length increases from the free ends towards the center in a continuous way and the central arm springs are not equivalent as it was the case close to equilibrium. Tension, again, clearly decreases towards the ends of the arms. The decrease of the spring tension as a function of its arm position is similar under shear and elongational flow, although under elongation that decrease seems slightly steeper (compare empty and black triangles) toward the end of the arm.

5. Summary

In this paper we have used the Brownian dynamics simulation technique applied to the bead-and-spring chain model to study the flow behavior of regular star polymers. Both in simple shear and uniaxial extensional flow, star polymers present a similar steady-state behavior to that of linear and ring polymers. Under both kind of flow, simulation results agree with the notion that tension builds up from the free ends to the center of the chain.

Under shear flow, the deformation of the star, δ^2, scales with the dimensionless shear rate, β, following the well-established quadratic power law $\delta^2 = C\beta^2$ for Gaussian chains. The inclusion of finite extensibility, excluded volume and hydrodynamic interaction tends to diminish slightly the exponent value, a kind of behavior also expected for linear polymers [26]. On other hand, in a log–log plot, the shear intrinsic viscosity is shown to present the classical behavior of polymer solutions: A Newtonian plateau at low shear rates and a power law decay at high shear rates, the so-called shear-thinning region. When excluded volume is present, the non-Newtonian regime starts with a soft decay in the viscosity before reaching the steep true shear-thinning region. When hydrodynamic interaction is included a soft shear thickening appears before the shear-thinning region. This behavior is predicted by theory [27] and simulation [5]. We find slopes in the shear-thinning region close to $-2/3$, in good agreement to some theoretical predictions [27].

Under elongational flow, star polymers present the

typical coil-stretch transition when the extensional rate exceeds a critical value $\dot{\varepsilon}_c$, analogously to the behavior presented by linear and ring chains. Indeed, there exists a similar power law for each topology relating the critical elongational rate with some characteristic molecular weight of the chain. They differ in that $\dot{\varepsilon}_c$ of linear and ring polymers scales with the total molecular weight, N, whereas for star polymers it scales with the arm molecular weight, N_{arm}. As found for linear and ring polymers, the power law depends on the presence of HI, in which case we find an exponent in between -1.5 and -1.6. Clearly, to get results comparable with experiments, HI must be considered in the simulations. Since the power laws relating τ_1 and $\dot{\varepsilon}_c$ of stars with N_{arm} present the same absolute exponent value just with opposite sign, the dimensionless quantity $\dot{\varepsilon}_c\tau_1$ can be easily computed, adopting a similar value to that found for linear polymers $\dot{\varepsilon}_c\tau_1 = 0.5$. In fact, linear and star chains of the same N_{arm} have similar longest relaxation time and similar critical elongational rate. Therefore, the product $\dot{\varepsilon}_c\tau_1$ seems to be independent of the topology.

Some limitations to the conclusions reported here can arise from the relatively small N values (no greater than 49) employed in our simulations. Small N implies small N_{arm} so that core effects become more relevant than when star arms are large. Thus, increase of core density makes HI and EV effects keep their importance when star is deformed by the flow. In addition, arms may not be fully in the large linear chain limit. This, for instance, may be a reason for our finding that the exponent of the power law giving the molecular weight dependence of the elongational rate is not exactly the same as that found for linear chains, increasing slightly with the presence of excluded volume potential. On other hand, as the number of arms increase the motion of the segments in the star core becomes increasingly difficult. For high F (usually greater than 6) arms stretch out even under unperturbed conditions which affects overall equilibrium properties if N_{arm} is not large enough [6].

Acknowledgements

This work has been supported by grant BQU2003-04517 from Dirección General de Investigación, MCYT. J.G.H.C. is the recipient of a Ramón y Cajal postdoctoral research contract. R.P. is the recipient of a predoctoral fellowship from MEC.

References

[1] De Gennes PG. J Chem Phys 1974;60:5030–42.
[2] Keller A, Odell JA. Colloid Polym Sci 1985;263:181–201.
[3] López Cascales JJ, Díaz FG, García de la Torre J. Polymer 1995;36:345–51.
[4] Hernández Cifre JG, García de la Torre J. J Rheol 1999;43:339–58.
[5] Hernández Cifre JG, Pamies R, López Martínez MC, García de la Torre J. Polymer 2005;46:267–74.
[6] Burchard W. Adv Polym Sci 1999;143:113–94.
[7] Rey A, Freire JJ, García de la Torre J. Macromolecules 1990;23:3948–53.
[8] Ganazzoli F, Fontelos MA, Allegra G. Polymer 1993;34:2615–22.
[9] Sikorski A, Romiszowski P. J Chem Phys 1998;109:6169–74.
[10] Freire JJ. Adv Polym Sci 1999;143:35–112.
[11] Hsu HP, Nadler W, Grassberger P. Macromolecules 2004;37:4658–63.
[12] Shida K, Ohno K, Kawazoe Y, Nakamura Y. Polymer 2004;45:1729–33.
[13] Mattice WL, Helfer CA. Polymer 2005;46:2389–94.
[14] Bird RB, Curtiss CF, Armstrong RC, Hassager O. Dynamics of polymeric liquids, kinetic theory. vol. 2. 2nd ed. New York: Wiley; 1987.
[15] Rey A, Freire JJ, García de la Torre J. Macromolecules 1987;20:342–6.
[16] Freire JJ, Rey A, García de la Torre J. Macromolecules 1986;19:457–62.
[17] Ermak DL, McCammon JA. J Chem Phys 1978;69:1352–60.
[18] Iniesta A, García de la Torre J. J Chem Phys 1990;92:2015–9.
[19] Rotne J, Prager S. J Chem Phys 1969;50:4831–7.
[20] Yamakawa H. J Chem Phys 1970;53:436–43.
[21] Öttinger HC. Stochastic processes in polymer fluids. Berlin: Springer; 1996.
[22] Batchelor GK. J Fluid Mech 1976;74:1–29.
[23] Carrasco B, García de la Torre J. J Chem Phys 1999;111:4817–26.
[24] López Cascales JJ, Navarro S, García de la Torre J. Macromolecules 1992;25:3574–80.
[25] Knudsen KD, Elgsaeter A, López Cascales JJ, García de la Torre J. Macromolecules 1993;26:3851–7.
[26] Knudsen KD, Elgsaeter A, García de la Torre J. Polymer 1996;37:1317–22.
[27] Ganazzoli F, Raffaini G. Macromol Theory Simul 1999;8:234–46.
[28] Pamies R, López Martínez MC, Hernández Cifre JG, García de la Torre J. Macromolecules 2005;38:1371–7.
[29] Menasveta MJ, Hoagland DA. Macromolecules 1992;25:7060–2.
[30] Narh KA, Odell JA, Keller A. J Polym Sci Polym Phys Ed 1992;30:335–40.
[31] Termonia Y. J Polym Sci Polym Phys Ed 2000;38:2422–8.
[32] Rabin Y, Henyey FS, Pathria RK. Phys Rev Lett 1985;55:201–3.